Electronic Supplementary Material (ESI) for Lab on a Chip

Supplementary information

In vitro angiogenesis assay for the study of cell-encapsulation therapy

Choong Kim,[ab] Seok Chung,[d] Liu Yuchun,[eh] Min-Cheol Kim,[b] Jerry K. Y. Chan,[efg] H. Harry Asada[bc] and Roger D. Kamm*[a bc]

Supplementary Methods

Computational modeling of concentration gradient and interstitial flow

Gradients of growth factors secreted by CE-beads, within the collagen scaffold were quantified by computational modeling using the coupled transient convection-diffusion and Brinkmann equations, which were solved using a commercial finite element solver, COMSOL (Burlington, MA).[1] In computational simulations, the growth factor diffusion coefficient in the scaffold was assumed to be 4.9×10^{-11} m^2/s.[2] Diffusion coefficients in the bead (2.2×10^{-10} m^2/s) and medium (6×10^{-11} m^2/s) were determined as previously described.[1, 3] Values of hydraulic permeability (scaffold = 10^{-13} m^2 and bead = 10^{-13} m^2) were selected based on those reported by Swartz et al.[1, 4] Growth factor secretion rates for cells in alginate beads were determined experimentally. Beads were modeled as a distributed source term (i.e., secreted growth factor source). Typical experimental values for the secretion rate of growth factor from a single cell (~ 0.006 pg/day), [5] and the number of encapsulated cells in a bead (~30) produced a total secretion rate of 8.85×10^{-11} $mol/m^3/s$. Interstitial flow, when applied, was created by imposing a pressure drop of 40 Pa between the central channel and the bead-trap region.

Particle simulation of CE-beads in microfluidic device

The motion of CE-beads in the microfluidic device was simulated using a coupled Lagrangian approach based on the pre-computed Newtonian flow fields. [6-9] The pre-computed flow field in the microfluidic device was computed using commercial computational fluid dynamics software (STAR-CD V4.12, CD-Adapco), with a finite volume code that allows for unstructured meshes of tetrahedral and prism elements. Computational models consisting of unstructured grids were generated with a single integrated package (STAR-CCM+ 6.04, CD-Adapco), and the steady-state flow field solution was optimized for a convergence of $\leq 10^{-6}$. The calculation interpolates the flow velocity and velocity gradients at the CE-bead's center of mass. A CE-bead was assumed to be a sphere with a radius (r_i^b) of 50 μm and to encapsulate about thirty spherical cells (N^c) with a radius (r^c) of 5 μm. Interactions between moving CE-beads were not considered because the suspension was of a sufficiently low concentration. However, interactions between a moving bead and stationary beads were considered to predict spatial distributions of packed CE-beads in trapping regions. Additionally, interactions with the channel's surface were considered to prohibit moving CE-beads from penetrating the computational wall boundary. The forces considered in the equation of translational motion for the *i*-th CE-bead were those due to the hydrodynamic drag, pressure gradient, gravity ($\left(m_i^b - m_i^f\right)\boldsymbol{g}$), Brownian motion ($\boldsymbol{F}_{B,i}^b$) and collisions between a moving bead and stationary beads ($\boldsymbol{F}_{S,i}^b$) and the surface ($\boldsymbol{F}_{W,i}^b$). So, the resulting six equations of translational motion equation for the *i*-th CE-bead are expressed as

$$m_i^b \frac{d\boldsymbol{v}_i^b}{dt} = \boldsymbol{F}_{D,i}^b + \boldsymbol{F}_{P,i}^b + \left(m_i^b - m_i^f\right)\boldsymbol{g} + \boldsymbol{F}_{B,i}^b + \boldsymbol{F}_{S,i}^b + \boldsymbol{F}_{W,i}^b, \quad i = 1, \cdots, N. \tag{1}$$

$$\frac{d\boldsymbol{x}_i^b}{dt} = \boldsymbol{v}_i^b \tag{2}$$

where $\boldsymbol{v}_i^b$ is the *i*-th CE-bead velocity, $\boldsymbol{x}_i^b$ is the location vector of the *i*-th CE-bead, and $F_{D,i}^b\left(=6\pi\eta r_i^b\left(\boldsymbol{v}_i^f - \boldsymbol{v}_i^b\right)\right)$ is the hydrodynamic drag force acting on the spherical bead under the Stokes flow regime. Here $\boldsymbol{v}_i^f$ stands for fluid velocity at the center of mass ($\boldsymbol{x}_i^b$), η is the dynamic viscosity of fluid (8.88×10^{-3} kg m^{-1} s^{-1}), and $m_i^b\left(=\frac{4\pi}{3}\left(\rho^b\left(r_i^b\right)^3 + N^c\left(\rho^c - \rho^b\right)\left(r^c\right)^3\right)\right)$ and $m_i^f\left(=\rho^f\frac{4\pi}{3}\left(r_i^b\right)^3\right)$ are the mean masses of the spherical CE-bead and fluid, respectively. Here ρ^b, ρ^c and ρ^f are alginate density (1040 kg m^{-3}), cell density (1080 kg m^{-3}) and fluid density (997.5 kg m^{-3}), respectively. N^c is the average number of encapsulated cells in a bead. $F_{P,i}^b\left(=m_i^f\frac{D\boldsymbol{v}_i^f}{Dt}\right)$ is the force due to the pressure gradient in the fluid surrounding the bead. Detailed mathematical expressions of $\boldsymbol{F}_{B,i}^b$, $\boldsymbol{F}_{S,i}^b$ and $\boldsymbol{F}_{W,i}^b$ are found elsewhere.[5, 6] N is the total number of seeded CE-beads.

The six ordinary differential equations (Eqs (1) and (2)) are solved using a fourth order Rosenbrock method based on an adaptive time-stepping technique as the integration method, as it was more reliable for solving stiff linear equations without divergence as compared to the Runge–Kutta method. In order to visualize the CE beads movement and flight times until their depositions occurring in the microfluidic device, time-lapse data were exported to a commercial plotting software package (Tecplot 360).

Supplementary References

1. I. K. Zervantonakis, S. Chung, R. Sudo, M. Zhang, J. L. Charest, and R. D. Kamm, *Intern J Micro-Nano Scale Transport*, 2010, **1**(1), 27-36.
2. C. L. E. Helm, M. E. Fleury, A. H. Zisch, F. Boschetti and M. A. Swartz, *PNAS*, 2005, **102**, 15779-15784.
3. S. Vériter, J. Mergen, R. M. Goebbels, N. Aouassar, C. Grégoire, B. Jordan, P. Levêque, B. Gallez, P. Gianello and D. Dufrane, *Tissue Eng Pt A*, 2010, **16**, 1503-1513.
4. M. A. Swartz and M. E. Fleury, *Annu Rev Biomed Eng*, 2007, **9**, 229-256.
5. H. Keshaw, A. Forbes and R. M. Day, *Biomaterials*, 2005, **26**, 4171-4179.
6. M. C. Kim, Z. H. Wang, R. H. W. Lam and T. Thorsen, *J Appl Phys*, 2008, **103**.
7. M. C. Kim and C. Klapperich, *Lab on a chip*, 2010, **10**, 2464-2471.
8. M. C. Kim, B. C. Isenberg, J. Sutin, A. Meller, J. Y. Wong and C. M. Klapperich, *Lab on a chip*, 2011, **11**, 1089-1095.
9. C. Kim, K. S. Lee, J. H. Bang, Y. E. Kim, M. C. Kim, K. W. Oh, S. H. Lee and J. Y. Kang, *Lab on a chip*, 2011, **11**, 874-882.
10. W. Saadi, S. J. Wang, F. Lin and N. L. Jeon, *Biomedical microdevices*, 2006, **8**, 109-118.

Supplementary Figures

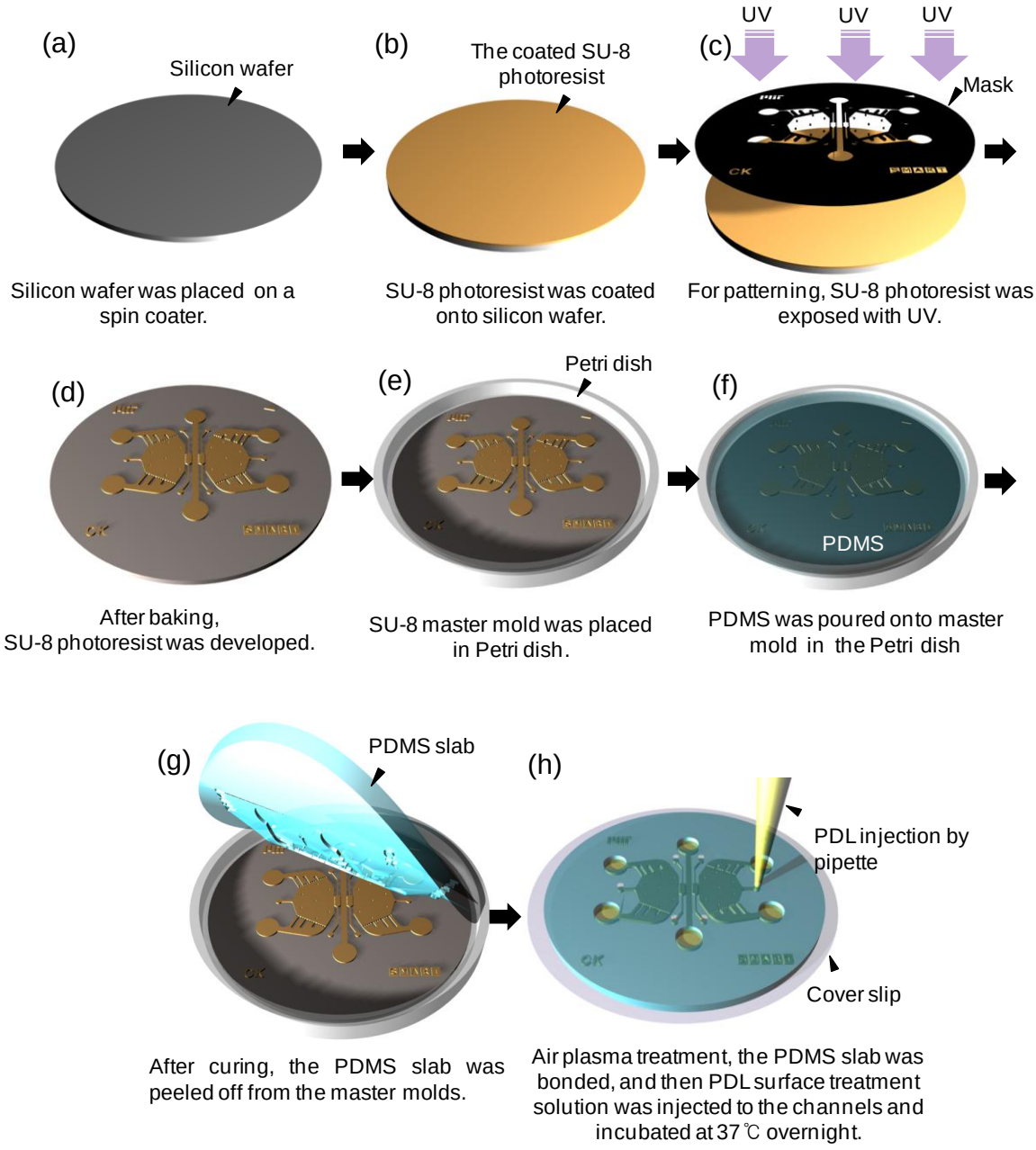

Figure S1. Preparation of the PDMS *in vitro* angiogenesis-on-a-chip

The chip was fabricated via conventional soft lithography (a–d), replica molding (e–g), and PDL coating (h). (a) A silicon wafer was placed on a spin coater to achieve the desired SU-8 resist film thickness. (b) SU-8 photoresist was coated onto the silicon wafer. (c) For patterning, the SU-8 photoresist on the silicon wafer was exposed to conventional UV (350-400 nm) radiation using a

photomask. (d) After baking and development, the SU-8 resist was developed with SU-8 developer, and an SU-8 master mold was made. (e) The SU-8 master mold was placed in a large Petri dish for PDMS preparation. (f) PDMS was poured onto the master mold in the Petri dish. (g) After curing, the PDMS replica was peeled away from the master mold. (h) After air plasma treatment for bonding, the PDMS slabs were bonded with a cover slip, then the PDL surface treatment solution was injected into the channels by pipette and the device was incubated at 37°C overnight.

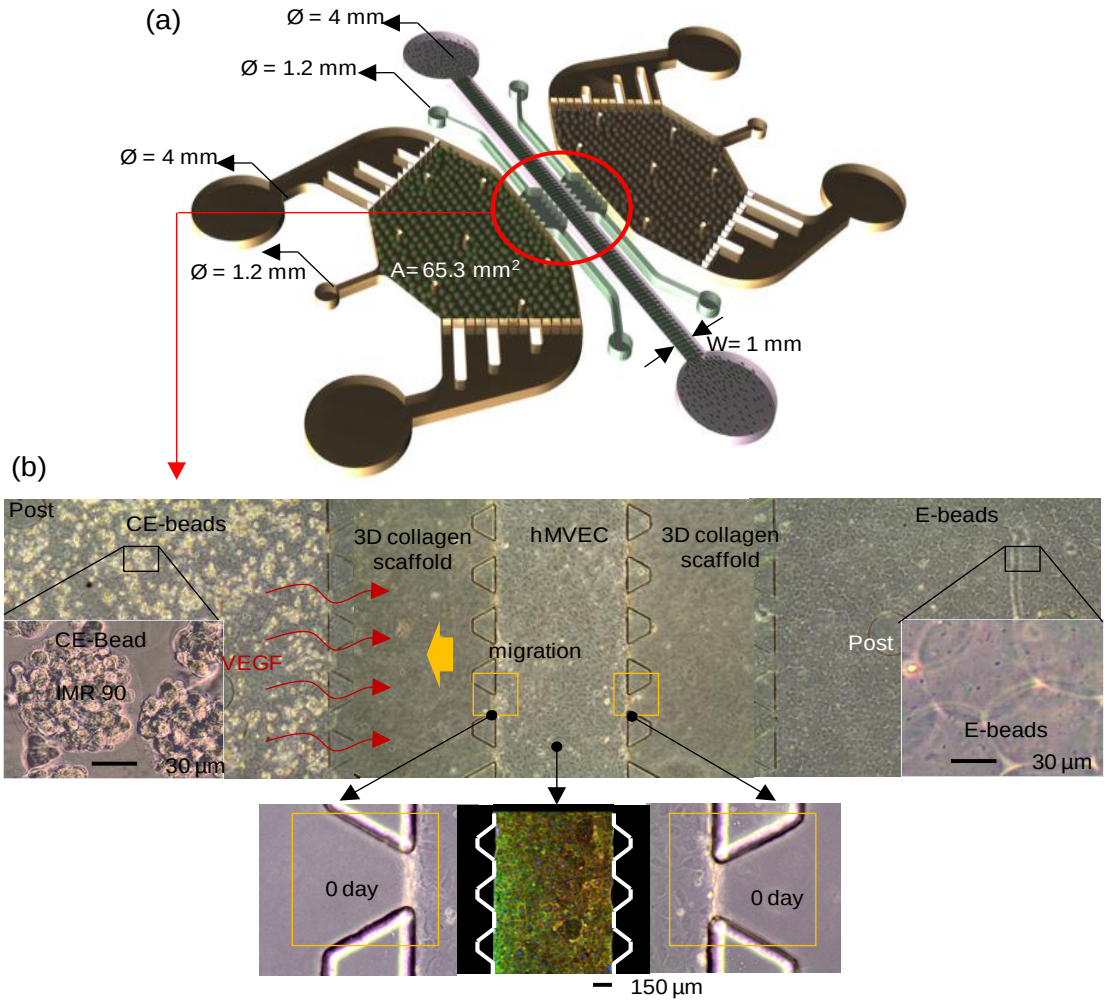

Figure S2. (a) Specifications and detailed views of the *in vitro* angiogenesis-on-a-chip system. The height of the chip is 120 µm. The width of the collagen gel region is 1.25 mm; each gel channel is partitioned using a series of regularly spaced posts (110 µm apart). Magnified view of the angiogenesis-on-a-chip platform, showing the three compartments: hydrogel (collagen) scaffold, central channel, and bead-trap regions. A difference of at least 6 ng/ml over a distance of 800 microns was needed to stimulate cell migration in the device.[10] We determined from our experiments that the IMR-90 fibroblasts secrete VEGF as a rate of 0.006 pg/day. Using this information in our computational model, we were able to ascertain that it was necessary to include ~7000 beads (at a cell density of 1.4×10^6 cells/ml) in the CE region in order to achieve the desired gradient. Circular-shaped posts (diameter = 300 µm) in the

bead-trap regions prevent the upper side of the trap region from sticking to the cover slip; square-shaped posts (distance between posts = 50 μm) are positioned to prevent beads from escaping the bead-trap region. (b) One day after seeding human microvascular endothelial cells, a confluent monolayer was formed in the central channel and cell-encapsulating beads (CE-beads) were introduced into the left side trap region with a syringe pump; empty beads without cells (E-beads) were introduced into the right side trap region to maintain mechanically symmetrical conditions.

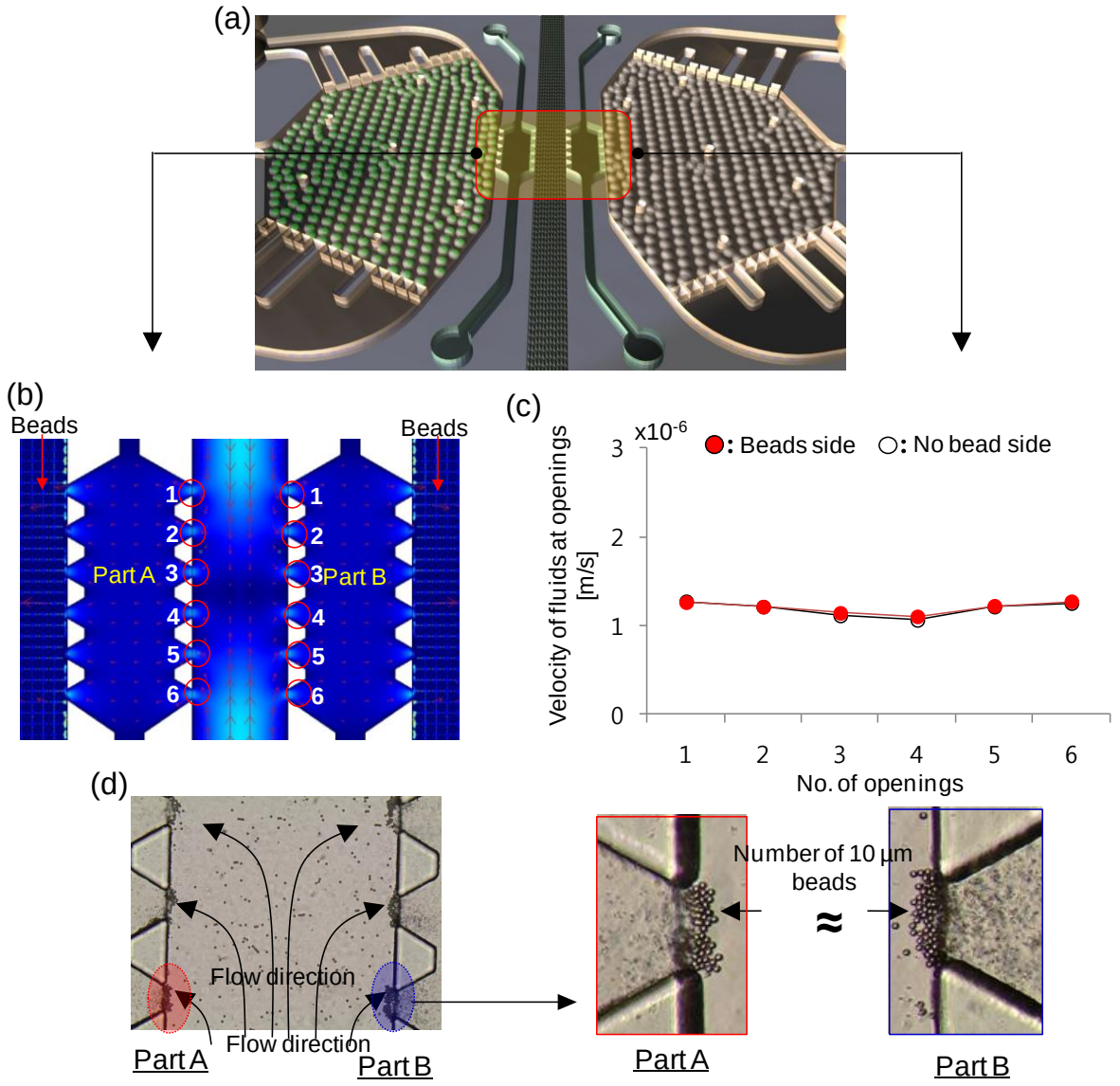

Figure S3. Hydrodynamic symmetry on both sides of the central channel. (a) Schematic view of the *in vitro* angiogenesis-on-a-chip system with CE-bead and E-bead conditions. Under these experimental conditions, the hydrodynamic resistances of both scaffold regions are the same because of their same material status, and the hydrodynamic resistances of both bead-trap regions are also the same owing to the presence of beads. (b) Simulated interstitial flow results, showing flow into each opening (Part A & B). (c) Graph showing velocities of fluids at the openings in part A and B. Injected fluid flowed with similar velocities toward the six openings in part A and B

because they have the same hydrodynamic resistances. (d) In these experiments, hydrodynamic symmetry was visualized by individually trapping CE-beads and E-beads in their respective sides. A similar number of beads collected on both sides (Part A and B) of the central channel, indirectly demonstrating a similar level of interstitial flow through the hydrogel scaffolds.

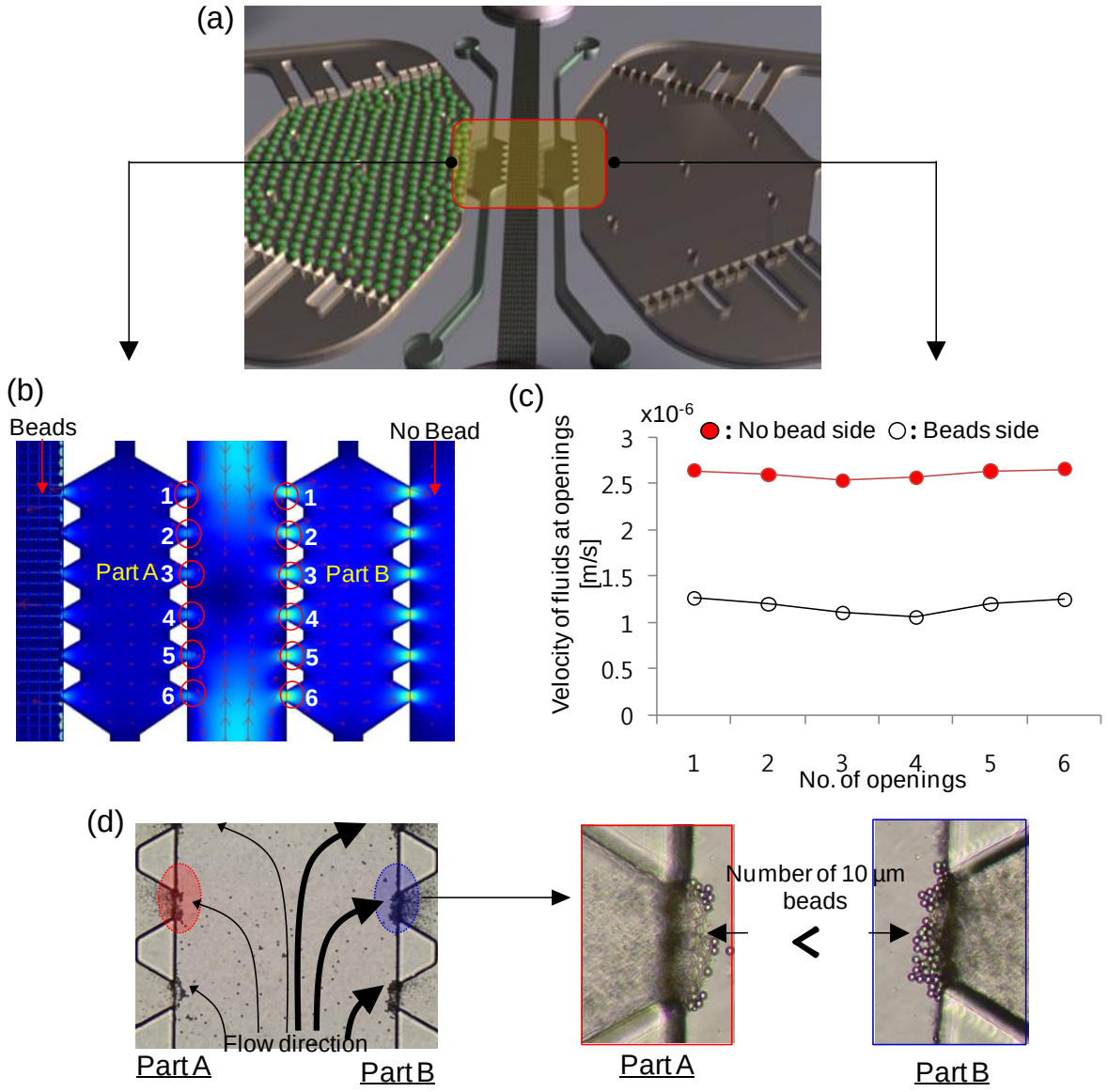

Figure S4. Hydrodynamic asymmetry on both sides of the central channel. (a) Schematic view of the *in vitro* angiogenesis-on-a-chip system with CE-bead and no bead conditions. Under these experimental conditions, the hydrodynamic resistances of both scaffold regions are the same because the material status of both regions is the same, but the hydrodynamic resistance of bead-trap regions are different, being much greater in the CE-beads region than in the no-beads condition on the right side. (b) Simulated interstitial flow results, showing flow into each opening (Part A & B).

(c) Graph showing velocities of fluids at the openings in part A and B. The velocity of fluid at the six openings in part B was twice as fast as that to part A because the hydrodynamic resistance of part A containing beads is much greater than that of part B. (d) Experimental strategy for verifying the difference in interstitial flow at both sides: First, CE-beads were injected only on the left side and 10-μm microbeads were introduced into the central channel, then trapped microbeads in each part were counted. Considerably more microbeads were trapped in part B without beads than part A. We conclude that presence of beads in trap regions can create a hydrodynamic imbalance.

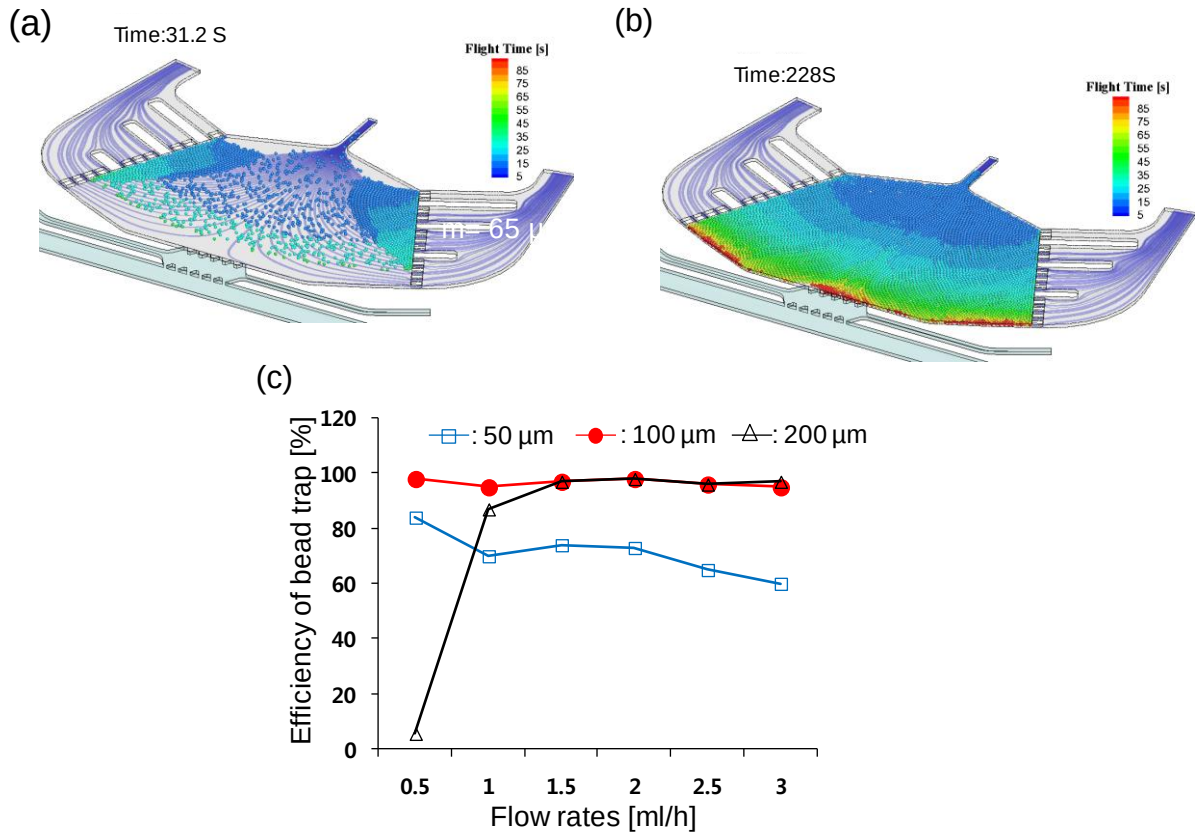

Figure S5. (a) Spatial distributions of simulated CE-beads in the trapping region after (A) 31.2 s and (b) 228 s of bead loading at the inlet; contour legend on spherical CE-beads indicates the elapsed time for an individual CE-bead travelling along the trapping region until its final deposition on the bottom substrate, and transparent blue ribbons represent streamlines along the trapping region. (c) Bead- trapping efficiency on the various diameters was evaluated when the bead diameters were varied as about 50 μm, 100 μm, and 200 μm. Beads of about 100 μm were the optimal size that allowed a bead- trapping efficiency of > 95 %. When small beads (D= 50 μm) were injected, trapping efficiency declined with increasing flow rates because small beads could escape through between the square-shaped posts spaced at 50 μm intervals due to its elasticity. For beads of ~ 200 μm, beads accumulation at the entrance was caused by low flow rates (> 0.5 ml/h) (bead- trapping efficiency: > 10%).

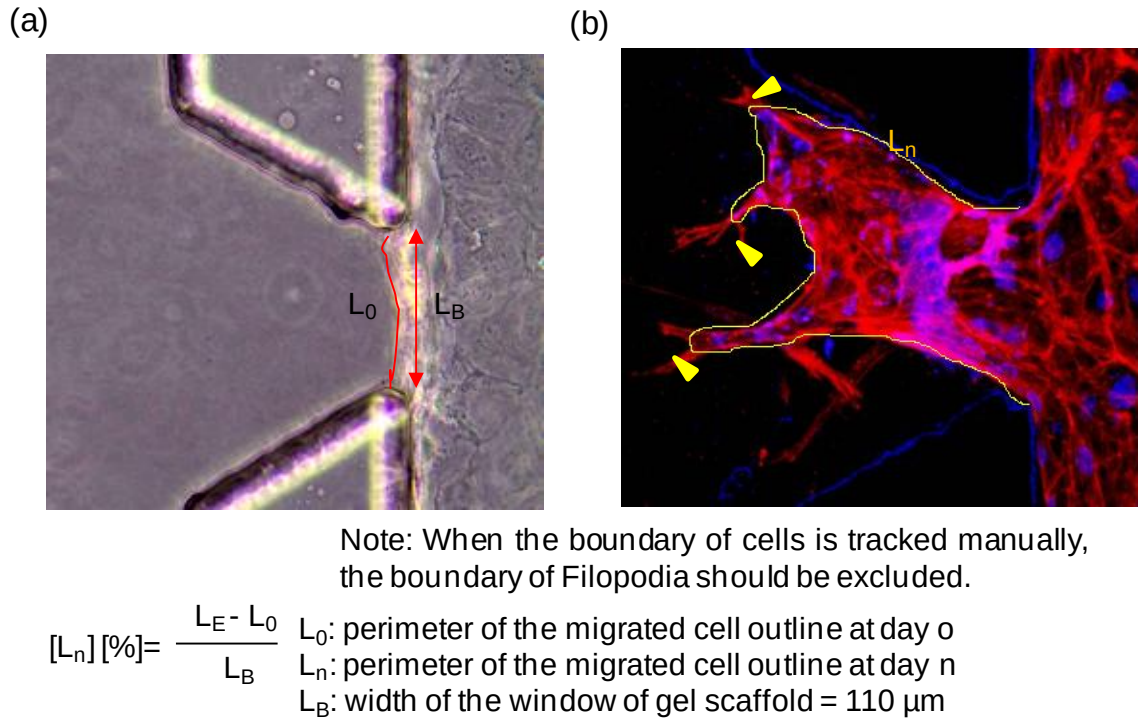

Figure S6. Quantification methods. Cell migration was monitored by phase-contrast microscopy and confocal microscopy. The boundary perimeter of the monolayer and the projected area of regions containing migrated cells were measured with Image J software. The cell boundary was tracked manually. (a) Initial perimeter (L_0) of endothelial cells; (b) endothelial cell perimeter on day

n (L_n). The data were then normalized to the corresponding values for the basic perimeter (LB) after subtracting the initial values (L_0). (c) Formation of a lumen greater than 100 μm; (d) formation of a lumen less than 100 μm. A lumen was defined as a structure with a length greater than 100 μm. Percent of lumen formation was measured relative to the total number in six openings.

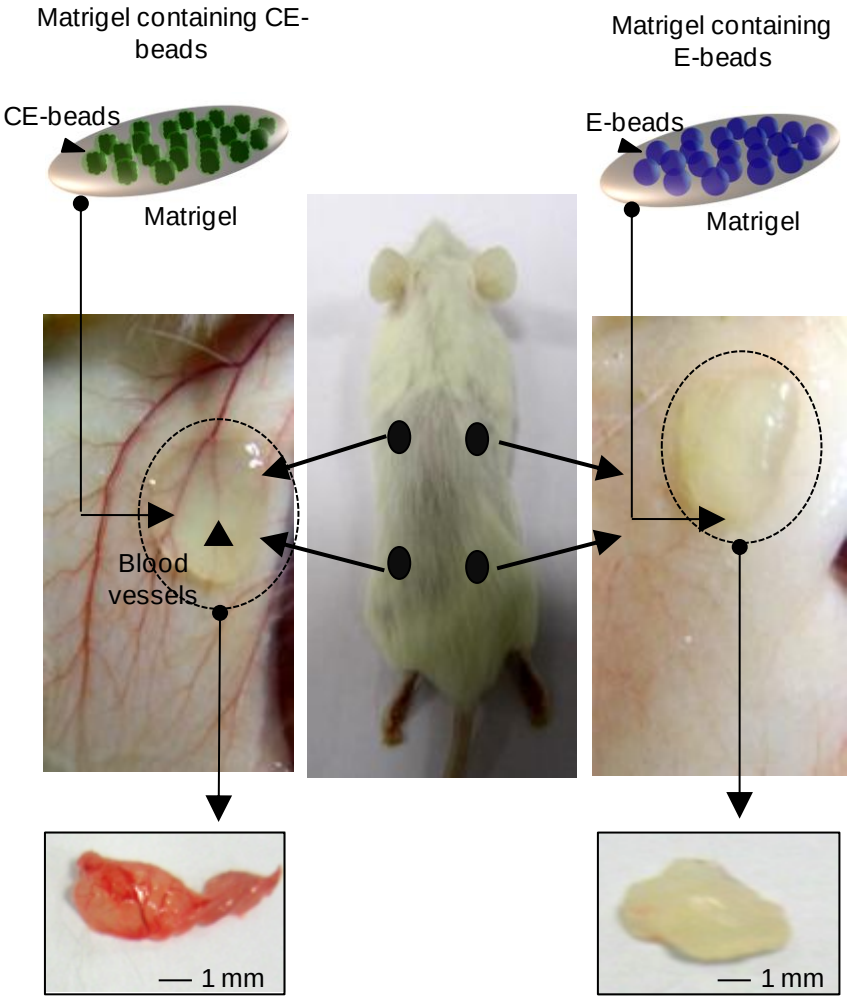

Figure S7. CE-beads in Matrigel were implanted subcutaneously into mice and maintained for 3 weeks. E-beads in Matrigel were used as a control.